Theor Chem Acc (2006) 115: 113–126
DOI 10.1007/s00214-005-0058-0

REGULAR ARTICLE

Jochen Blumberger · Michiel Sprik

Quantum versus classical electron transfer energy as reaction coordinate for the aqueous Ru^{2+}/Ru^{3+} redox reaction

Received: 13 August 2004 / Accepted: 6 October 2005 / Published online: 10 December 2005

Abstract Applying density functional theory (DFT)-based molecular dynamics simulation methods we investigate the effect of explicit treatment of electronic structure on the solvation free energy of aqueous Ru^{2+} and Ru^{3+}. Our approach is based on the Marcus theory of redox half reactions, focussing on the vertical energy gap for reduction or oxidation of a single aqua ion. We compare the fluctuations of the quantum and classical energy gap along the same equilibrium ab initio molecular dynamics trajectory for each oxidation state. The classical gap is evaluated using a standard point charge model for the charge distribution of the solvent molecules (water). The quantum gap is computed from the full DFT electronic ground state energies of reduced and oxidized species, thereby accounting for the delocalization of the electron in the donor orbital and reorganization of the electron cloud after electron transfer (ET). The fluctuations of the quantum ET energy are well approximated by gaussian statistics giving rise to parabolic free energy profiles. The curvature is found to be independent of the oxidation state in agreement with the linear response assumption underlying Marcus theory. By contrast, the diabatic free energy curves evaluated using the classical gap as order parameter, while also quadratic, are asymmetric reflecting the difference in oxidation state. The response of these two order parameters is further analysed by a comparison of the spectral density of the fluctuations and the corresponding reorganization free energies.

Keywords Redox reactions · Marcus theory · Energy gaps · Ab initio molecular dynamics simulation · Ru aqua cations

1 Introduction

A crucial element in the Marcus theory of electron transfer (ET) [1–4] is the simple and effective treatment of the polar solvent. Solvation is accounted for by two intersecting parabolic free energy curves, one for the reactant, and one for the product state. The reaction coordinate controlling the free energy is the polarization of the solvent induced by the charge carried by the donor and acceptor solute. In the original formulation of the theory [1] the polarization was described by the linear response of a dielectric continuum. The linear response assumption not only justifies the quadratic dependence on the reaction coordinate but also implies that the curvatures of the parabola could be taken to be identical. The entire solvent effect could thus be summarized in a single parameter, the reorganization free energy (traditionally denoted by λ) appearing in the famous gap law for the activation free energy. Marcus also derived a compact expression for λ using a dielectric cavity model allowing for more quantitative predictions (For recent reviews see Refs. [5,6]; Ref. [4] is a more personal review with a historical perspective).

The success and simplicity of Marcus theory posed both a challenge and opportunity for computer simulation. The semiclassical approach of Marcus theory, separating the electronic structure of the donor (D) and acceptor (A) from the classical motion of the solvent, meant that a number of predictions and assumptions could be tested using classical force field-based molecular dynamics methods. This rather ingenious direction in computational chemistry was pioneered by Warshel and coworkers [7–9] and subsequently extended by numerous other groups [10–27]. A first important question that was investigated was the validity of the parabolic approximation of the free energy surface. This required a precise microscopic definition of the polarization order parameter, for which Warshel took the vertical energy gap [8]. This definition, already anticipated in an early paper of Marcus [2], is a most natural choice for a reaction coordinate for nonadiabatic ET. It follows from the golden rule in the limit of a classical treatment of the ionic motion and is a direct consequence of the Franck–Condon approximation. Simulations of model aqueous self-exchange reactions verified that the diabatic free energy surfaces are indeed quadratic to a very good accuracy. As an example we mention the popular aqueous Fe^{3+}/Fe^{2+} system, which has been investigated repeatedly using various force field models. Deviations from linear response were found to be small (<10%) both for

J. Blumberger · M. Sprik(✉)
Department of Chemistry, University of Cambridge,
Cambridge CB2 1EW, United Kingdom
E-mail: ms284@cus.cam.ac.uk

the homogeneous self-exchange reaction $Fe^{*3+} + Fe^{2+} \rightarrow Fe^{*2+} + Fe^{3+}$ [10,9,14,24]as for the heterogeneous $Fe^{3+} + e^- \rightarrow Fe^{2+}$ redox reaction in the proximity of an electrode surface [12,13,16,18].

The reactant and product free energy surfaces are assumed to have the same curvature in Marcus theory. This property is necessarily satisfied for self-exchange reactions even if the polarization of the solvent is not strictly linear. Charge separation ($D + A \rightarrow D^+ + A^-$) and the reverse charge recombination reaction ($D^+ + A^- \rightarrow D + A$) are in this respect a more critical test. Indeed charge recombination reactions can show in the inverted region a dependence on the free energy gap differing significantly from the approximately parabolic dependence in the normal region. While some of these nonlinearities can be explained by quantum motion of intramolecular modes of the solute (molecule or complex, see e.g. Ref. [5]), Kakitani and Mataga [28,29] suggested that also dielectric saturation could play a role. Carter and Hynes [11] tested this possibility in a classical simulation study of a charge separation/recombination reaction (ignoring all quantum effects) and in fact obtained a significantly different second moment for the vertical gap fluctuations of the (equilibrium) neutral and ion pair. Converting these gap fluctuations to reorganization free energies using the relation between these quantities in the linear regime led to an asymmetric gap law in disagreement with Marcus theory and seemingly supporting the Kakitani and Mataga hypothesis.

The apparent conflict with Marcus theory was resolved by Tachiya [30] who showed, using rigorous statistical mechanical arguments, that a difference in second derivative of reactant and product state is incompatible with a parabolic shape of the energy curves and must be the result of nonlinear behaviour. This was confirmed by King and Warshel [9] who using thermodynamic perturbation methods extended the range of nonequilibrium gap values for the same model used in Ref. [11]. In this way they were able to show that higher-order terms are vital in fitting the free energy curves. Moreover, the extended free energy curves were found to be considerably more similar than suggested by the extrapolation based on the second-order derivative at the equilibrium gap value, leading in turn to far less pronounced asymmetries in the gap law.

The discussion about nonlinearity and corresponding asymmetries in the gap law has been recently revived by Matyushov and Voth who identified a further source of nonlinear response, namely a possible dependence of the solute polarizability on the oxidation state [31]. This property is missing in Marcus' formulation of ET and most classical force field models. Matyushov and Voth investigated the implications of this effect in an analytic study of a two-state–one mode vibronic model with an electronic state-dependent curvature of the two diabatic harmonic potential energy surfaces. The significant distortion of the Marcus gap law that could be achieved by this model was subsequently verified by simulation of a classical polarizable solute [21].

Heterogeneous ET is an example of electron exchange between two profoundly inequivalent reactants: the redox active solute undergoes a drastic change when oxidized or reduced while the metal electrode is hardly affected at all. Similar to charge recombination, electrode processes could therefore provide information about the effect of solute polarization. In fact, as pointed out by Marcus [3], the variation of the logarithm of the current with overpotential (after the electrochemist have applied their corrections for transport) is a good probe of possible gap relations. This is nicely illustrated by the derivation of the Butler–Volmer equation as presented in textbooks on electrochemistry (see for example Ref. [32]). The effect of an electrode is, in first instance, reduced to a variable shift of the potential (and free) energy surface of the oxidized state of the solute with respect to the reduced state. Any asymmetry in the gap law is in this picture entirely the result of a difference in curvature (or rather shape) of the free energy surface of the oxidation states of the solute in homogeneous solution (no physical electrodes present).

This picture is also the philosophy behind the ab initio molecular dynamics ("Car–Parrinello") simulation method we have developed for the study of electrochemical half reactions. The method was applied in the study of a number of redox half reactions involving transition metal aqua ions (Cu^+/Cu^{2+} in Ref. [33], Ag^+/Ag^{2+} in Refs. [33,34], Ru^{2+}/Ru^{3+} in Ref. [35], MnO_4^-/MnO_4^{2-} and RuO_4^-/RuO_4^{2-} in Ref. [36]). Changes in electronic structure upon oxidation are appreciable in these compounds. The fairly accurate agreement with experiment for the redox potentials of full redox reactions [33,36] gives some confidence that density functional theory (DFT) can be relied on to describe these effects suggesting that our approach could be used to subject the Matyushov–Voth conjecture to a numerical test. In particular the ruthenium hydrate half reaction [35] is of interest:

$$Ru^{3+} + e^- \longrightarrow Ru^{2+}. \quad (1)$$

These ions have the same electronic *d* shell configuration and core charge as Fe^{3+} and Fe^{2+}, but unlike iron ions are low spin avoiding certain technical complications in the density functional treatment used in the ab initio MD method. In Ref. [35] we computed the diabatic free energy profiles for the single aqua ions Ru^{3+} and Ru^{2+} using constrained and unconstrained Car–Parrinello MD. We used the same order parameter as in previous force field-based calculations [9,10, 12–14,24] namely the classical solvent electrostatic potential at the site of the ion evaluated by assigning fixed point charges to solvent atoms. It was found that both diabatic curves are well approximated by parabolae but the curvature of Ru^{3+} was almost twice as large as for Ru^{2+}. An asymmetry of this size seems to contradict the classical model simulation result reported by Rose and Benjamin [12] who found only minor deviations for the redox couple Fe^{3+} and Fe^{2+}.

The results of the calculation of Ref. [35] could therefore be interpreted as support for the Matyushov–Voth effect. However, while the electrostatic potential experienced by an ion in a simple point charge model can be equated to the vertical energy gap, this is not allowed in an explicit electronic structure calculation. An interesting question therefore, and focus of this work, is how the shape of the free energy profiles

changes if the true electronic vertical energy gap is used as a reaction coordinate rather than the classical solvent electrostatic potential. The quantum ET energy takes into account the delocalization of the electron in the donor orbital and electronic relaxation after ET, effects which are missing in the classical coordinate. This was also at the heart of the argument of Matyushov and Voth, which would suggest that differences in curvature of free energy profiles can only be enhanced in a consistent quantum treatment of the polarization. Here we address this issue by comparing the probability distributions of quantum and classical ET energy for the diabatic states involved. Anticipating our results, we find that the quantum gap fluctuations are again gaussian, but contrary to the classical electrostatic order parameter, give parabolic free energy curves with virtually identical curvature in the two oxidation states, thus closely adhering to Marcus theory, begging the question how the solvent compensates for the difference in oxidation state of the ions. To gain some microscopic insight in the ET mechanism we have performed a structural and dynamical analysis relating fluctuations of ET energy to fluctuations of structure. The idea is to identify the relevant motions of the solvated coordination complex that drive the ET reaction and compare how they are reflected in the classical and quantum order parameter fluctuations. This analysis also enables us to compare our ab initio molecular dynamics results for aqueous Ru^{2+}/Ru^{3+} to structural and dynamical data from experiment and simulation studies of other metal cation hexahydrates, in particular Al^{3+}, [37–39] Fe^{3+}, [40], and Cr^{3+}, [41].

This paper is organized as follows. In Sect. 2 we review the predictions of Marcus theory and then define the quantities related to MD simulation: quantum and classical ET energy, the corresponding probability distributions and spectral density functions. It is shown how the free energy profile for homogeneous ET between two infinitely separated ions can be calculated from the profiles for heterogeneous ET. In Sect. 3 we present radial distribution functions of aqueous Ru^{3+} and Ru^{2+} obtained from Car–Parrinello MD. Free energy profiles for heterogeneous and homogeneous ET are discussed and compared to the predictions of Marcus theory. Solvent effects are investigated by comparing the results obtained for aqueous solutions with the data obtained for the gas phase. Spectra of the time correlation function (TCF) of the ET energy fluctuations are presented and discussed. Section 4 is a discussion and conclusion.

2 Theory and method

2.1 Reorganization free energies and order parameter fluctuations

Electron transfer is an example of a chemical reaction which can be treated in the diabatic representation as defined by a full set of diabatic potential energy surfaces, one for the reactant (denoted by A) and one for the product (denoted by B). Such a two-surface picture allows for the introduction of reorganization free energy, which, as the success of the Marcus theory shows, is a particularly powerful concept for the understanding of a chemical process. We will follow the statistical mechanical formulation of Warshel, first presented in Ref. [7] and applied and reviewed in many subsequent publications (see for example Ref. [9]). The key equations required for the analysis of our results are summarized below.

Reorganization free energy quantifies the decrease in free energy following a vertical ET. Similar to activation free energy it depends on the specification of a suitable reaction coordinate ξ describing the nonequilibrium states along the reaction path. In a statistical mechanical treatment ξ must be formally defined in terms of a function $\xi\left(\mathbf{R}^N\right)$ of the microscopic configuration $\mathbf{R}^N$ (i.e. the coordinates of all N atoms of the system). ξ can be the solvent polarization as in the original Marcus theory, or a geometric quantity or the vertical energy gap ΔE itself:

$$\Delta E(\mathbf{R}^N) = E_{\mathrm{B}}(\mathbf{R}^N) - E_{\mathrm{A}}(\mathbf{R}^N), \tag{2}$$

where $E_M\left(\mathbf{R}^N\right), M = \mathrm{A,B}$ are the diabatic potential energy surfaces. Once the reaction coordinate is decided we can obtain the microscopic expression for the corresponding diabatic (Landau) free energy functions A_M, $M = \mathrm{A,B}$ in the form of a constrained partition function.

$$A_M(\xi') = -k_{\mathrm{B}}T \ln \Lambda^{-3N} \int \mathrm{d}\mathbf{R}^N \exp[-\beta E_M\left(\mathbf{R}^N\right)]\delta\left(\xi\left(\mathbf{R}^N\right) - \xi'\right), \tag{3}$$

where Λ is the average thermal wavelength, $T = 1/(k_{\mathrm{B}}\beta)$ the temperature, k_{B} the Boltzmann constant, δ the Dirac delta function. The connection to order parameter fluctuations is made by introducing the probability distribution:

$$p_M(\xi') = \frac{\int \mathrm{d}\mathbf{R}^N \exp[-\beta E_M\left(\mathbf{R}^N\right)]\delta(\xi(\mathbf{R}^N) - \xi')}{\int \mathrm{d}\mathbf{R}^N \exp[-\beta E_M\left(\mathbf{R}^N\right)]}. \tag{4}$$

The free energy function of Eq. (3) can then be separated in the logarithm of $p_M(\xi')$ which can be sampled from a simulation:

$$A_M(\xi') = -k_{\mathrm{B}}T \ln p_M(\xi') + A_M, \tag{5}$$

and the (diabatic) free energy

$$A_M = -k_{\mathrm{B}}T \ln \Lambda^{-3N} \int \mathrm{d}\mathbf{R}^N \exp[-\beta E_M\left(\mathbf{R}^N\right)]. \tag{6}$$

which can be determined (relative to a reference state) by thermodynamic perturbation methods.

These completely general relations, valid for any set of diabatic energy surfaces, lead to a formal definition of a reorganization free energy λ_{A} for the reactant and λ_{B} for the product state

$$\lambda_{\mathrm{A}} = A_{\mathrm{A}}(\xi_{\mathrm{B}}) - A_{\mathrm{A}}(\xi_{\mathrm{A}}) \tag{7}$$

$$\lambda_{\mathrm{B}} = A_{\mathrm{B}}(\xi_{\mathrm{A}}) - A_{\mathrm{B}}(\xi_{\mathrm{B}}), \tag{8}$$

where ξ_M is the expectation value of the reaction coordinate in state $M = \mathrm{A,B}$

$$\xi_M = \left\langle \xi\left(\mathbf{R}^N\right)\right\rangle_M = \int d\xi'\, \xi'\, p_M\left(\xi'\right). \tag{9}$$

The subscripted angular brackets indicate a canonical average over potential energy surfaces $E_M\left(\mathbf{R}^N\right)$.

The region in the configuration space occupied by the reactant state generally represents a highly unstable nonequilibrium state of the product. The evaluation of reorganization free energy requires, therefore, extensive application of special sampling methods such as the weighted histogram scheme (see Ref. [9]). However, in the linear regime, assumed by Marcus theory, the reorganization free energies can be directly obtained from the variance of equilibrium fluctuations of the order parameter by means of a quadratic extrapolation of the free energy profiles [Eq. (5)]. Using a notation similar to Eq. (9) the variance (second moment) of the order parameter can be written as

$$\sigma_M^2 = \left\langle \left(\delta\xi\left(\mathbf{R}^N\right)\right)^2 \right\rangle_M = \int d\xi' \, \left(\xi' - \xi_M\right)^2 \, p_M\left(\xi'\right), \quad (10)$$

and the corresponding linear response reorganization free energy is given by

$$\lambda'_M = \frac{k_\mathrm{B}T}{2\sigma_M^2}\left(\xi_\mathrm{A} - \xi_\mathrm{B}\right)^2. \quad (11)$$

A rather special situation arises however when the vertical energy gap ΔE of Eq. (2) is used as the reaction coordinate, $\xi = \Delta E$. Inserting Eq. (2) in Eq. (3) it can be shown [7,30, 42] that the corresponding free energy profiles are related by

$$A_\mathrm{B}(\Delta E) - A_\mathrm{A}(\Delta E) = \Delta E. \quad (12)$$

It is therefore sufficient to compute the free energy curve of one diabatic state, say A. The corresponding curve for state B is then found by adding the energy gap to the curve computed for A [30]. For parabolic free energy curves this leads to a drastic simplification: in order for Eq. (12) to be fulfilled the curvatures, reorganization free energies and widths of the gaussian distributions of states A and B must be equal:

$$\lambda_\mathrm{A} = \lambda_\mathrm{B} =: \lambda \quad (13)$$

$$\sigma_\mathrm{A} = \sigma_\mathrm{B} \quad (14)$$

$$\xi_\mathrm{A} = \lambda + \Delta A \quad (15)$$

$$\xi_\mathrm{B} = -\lambda + \Delta A, \quad (16)$$

where $\Delta A = A_\mathrm{B} - A_\mathrm{A}$ is the reaction free energy change (for a derivation of Eqs. (13),(14),(15) and (16) see for example Ref. [36]). Curvature, horizontal and vertical relative position of the minima of the two free energy curves are therefore entirely determined by only two parameters, the reorganization free energy λ and the thermodynamic driving force ΔA. Then assuming with Marcus that the ET takes place at the crossing point of the two quadratic diabatic curves (Franck–Condon principle) we obtain the Marcus gap law

$$\Delta A^\ddagger = \frac{(\lambda + \Delta A)^2}{4\lambda}, \quad (17)$$

relating the free energy barrier $\Delta A^\ddagger$ to the ET driving force ΔA. Eqs. (13),(14),(15) and (16) have also consequences for the reorganization free energies defined via the gap fluctuations according to Eq. (11)

$$\lambda'_\mathrm{A} = \frac{\beta}{2}\langle\delta\Delta E\rangle^2_\mathrm{A} \quad (18)$$

$$\lambda'_\mathrm{B} = \frac{\beta}{2}\langle\delta\Delta E\rangle^2_\mathrm{B}, \quad (19)$$

where $\langle\delta\Delta E\rangle_M = \langle\Delta E - \Delta E_M\rangle_M$. Because the variance of the fluctuations is independent of the oxidation state [Eq. (14)] the reorganization free energies of Eqs. (11), (18) and (19) are again equal and identical to λ

$$\lambda'_\mathrm{A} = \lambda'_\mathrm{B} = \lambda. \quad (20)$$

Equation (20) seems to be a surprising result because λ, respectively, λ_M [Eqs. (7), (8)] and λ'_M [Eqs. (18), (19)] are in principle quite different quantities (which is why we have distinguished them by an accent). The latter is determined by the motion on a single diabatic PES while the former seemingly refers to two energy surfaces. We want to emphasize here that Eqs. (20),(13),(14),(15),(16),(17), (18) and (19) are entirely a consequence of using the ET energy as the reaction coordinate in combination with the assumption of gaussian statistics for this coordinate. These relations do not hold if the ET is described by a reaction coordinate other than the ET energy (e.g. bond length or a path in a two-dimensional space spanned by ET energy and a geometrical coordinate). Only in the very special case of ET energy the order parameter distribution of one diabatic state determines the distribution of the other diabatic state, and therefore both distributions can be described by a single parameter which is the reorganization free energy λ.

2.2 Heterogeneous electron transfer to a virtual electrode

Two types of ET reactions A $\longrightarrow$ B are distinguished: homogeneous ET reactions between a donor and an acceptor both solvated in the same medium and heterogeneous ET reactions between a solvated ion and an electrode E. In the first case A denotes the donor–acceptor complex D–A before the ET and B the complex D^+–A^- after the transfer. In the second case A stands for a system consisting of a single solvated ion in the reduced state R in contact with an electrode E (A = R+E) and B the ion in the oxidized state O and the excess electron located on E (B = O+E^-). An advantage of studying heterogeneous over homogeneous ET reactions is that the thermodynamic driving force can be controlled by variation of the electrode potential. This is particularly straightforward in the most elementary model of an electrode process (see for example Ref. [32]) in which the electrode is replaced by an electron reservoir containing electrons at an electronic chemical potential μ which, however, has no physical interactions with the ionic solution. The computational method we used in Refs. [33],[35] can be viewed as an MD implementation of this virtual electrode model in a finite periodic cell. As we argue in Ref. [35], the μ in our model can still be interpreted as an electrode potential ϵ (in atomic units) even though the reference electrode is completely artificial (see also Ref. [43]).

The net effect of this fictitious noninteracting electrode is a shift of the PES of O by μ adding to the vertical energy gap ΔE of Eq. (2):

$$\Delta E_\mu := E_\mathrm{B} - E_\mathrm{A} = \Delta E_0 + \mu. \tag{21}$$

ΔE_0 is the ET energy at zero electronic chemical potential which we refer to as ionization energy (electron affinity) if state R (O) generates the ion dynamics,

$$\Delta E_0(\mathbf{R}^N) = E_\mathrm{O}(\mathbf{R}^N) - E_\mathrm{R}(\mathbf{R}^N). \tag{22}$$

E_O and E_R are the ground state PESs of O and R, respectively. The free energies A_M of Eq. (6) are affected in exactly the same way leading to a reaction free energy offset by μ.

$$\Delta A_\mu := A_\mathrm{B} - A_\mathrm{A} = \Delta A + \mu. \tag{23}$$

ΔA_μ is the driving force of ET and ΔA the "unbiased" oxidation free energy difference $\Delta A = A_\mathrm{O} - A_\mathrm{R}$ at $\mu = 0$.

ΔA can "in principle" be computed from molecular dynamics simulation using the free energy perturbation formula [42] applied to state R and O,

$$\Delta A = -\frac{1}{2} k_\mathrm{B} T \ln \frac{\langle \exp(-\beta \Delta E_0) \rangle_\mathrm{R}}{\langle \exp(\beta \Delta E_0) \rangle_\mathrm{O}}. \tag{24}$$

In practice such exponential averages are rather difficult to evaluate unless there is substantial overlap between the two regions in configuration space accessible by equilibrium thermal fluctuations. In our previous study [35] we have shown that these conditions are actually met for the $Ru^{2+} \rightarrow Ru^{3+} + e^-$ half reaction. We compared diabatic free energy profiles [Eq. (5)] computed using constrained and equilibrium ab initio MD simulation. The same order parameter was employed as in classical simulations namely the solvent electrostatic potential ϕ at the site of the metal ion as determined from a point charge model,

$$\phi\left(\mathbf{R}^N\right) = \sum_{\mathbf{n}} \sum_{I=2}^{N} \frac{q_I}{|\mathbf{R}_I + \mathbf{n}L - \mathbf{R}_1|} \tag{25}$$

In Eq. (25) q_I denotes the charge of atom I at position $\mathbf{R}_I$, the Ru ion is labelled 1, H and O atoms from 2 to N, L is the box length and $\sum_{\mathbf{n}}$ stands for lattice summation. In our DFT simulation ϕ was treated merely as an order parameter for reversible transformation between redox states. In a classical point charge model, however, the solvent potential ϕ of Eq. (25) is directly related to the vertical energy gap of Eq. (2) as noted by Warshel in his pioneering work on modelling of ET reactions [7]. For clarity, classical (point charge) energy gaps will be indicated by ΔU while the notation ΔE will be reserved for quantum gaps computed using electronic structure methods.

For homogeneous reactions ΔU can be taken identical to the difference in the value of ϕ at the site of the donor and acceptor ion (in atomic units), ignoring further electronic contributions. Of course for single ions the missing electronic term, in first approximation equal to the vacuum ionization energy, is not at all small and is in fact of similar magnitude as the electrostatic potential ϕ ($\approx$ the difference in hydration energy of the two oxidation states) but of opposite sign. For the purpose of comparison to a fully consistent DFT calculation of a half reaction it is therefore convenient to "calibrate" ΔU by the ionization energy in vacuum, denoted by ΔE_0^v, leading to the following expression for the classical vertical gap,

$$\Delta U(\mathbf{R}^N) = e\phi(\mathbf{R}^N) + \frac{\xi_\mathrm{EW}}{2L}(q_\mathrm{O}^2 - q_\mathrm{R}^2) + \Delta E_0^\mathrm{v} \tag{26}$$

where e is the elementary charge. We have also included the self- interaction energy of the ion with its periodic images and background charge in a finite periodic cell [44]. The Ewald constant $\xi_\mathrm{EW} = -2.837297$ and L is the box length. q_M is the classical point charge of the ion in state M. For the $Ru^{2+} \rightarrow Ru^{3+} + e^-$ reaction of interest here $q_\mathrm{O}^2 - q_\mathrm{R}^2 = 9 - 4 = 5$. Similar to Eq. (21) we can again bias the gap by the electronic chemical potential μ,

$$\Delta U_\mu(\mathbf{R}^N) = \Delta U(\mathbf{R}^N) + \mu, \tag{27}$$

so that ΔU_μ can be interpreted as the energy required to transfer the electron from the site of the ion to the electrode within a classical model for ionic solvation. Note that in Eqs. (27) and (26) all terms except $\phi(\mathbf{R}^N)$ are constants. Therefore the free energy profiles along ΔU_μ, $A_M(\Delta U_\mu)$, are only shifted horizontally wrt. the profiles along ϕ leaving fluctuations and curvature unchanged.

Although the free energy profiles along ϕ (and therefore along ΔU_μ) were found to be well approximated by parabolae, the curvature for the oxidized state was almost twice as large as for the reduced state and similarly for the reorganization free energies we obtained $\lambda_\mathrm{O} \approx 2\lambda_\mathrm{R}$. This observation is not in conflict with the results of linear response theory (see Sect. 2.1) according to which $\lambda_\mathrm{O} = \lambda_\mathrm{R} := \lambda$ [Eq. (13)] if the fluctuations of the ET energy are gaussian. The reason is that ΔU_μ is *not* the ET energy in an ab initio MD simulation as opposed to classical MD. The relevant energy is now the full vertical quantum gap ΔE_μ of Eq. (21). The objective of this work is to verify whether the fluctuations of ΔE_μ are gaussian, or, equivalently, whether the linear response assumption holds for the Ru^{2+}/Ru^{3+} redox couple.

Total energies E_R and E_O are calculated at the level of DFT for a single solvated ion in periodic boundary conditions. Hence, the difference, ΔE_μ can be viewed as the quantum equivalent of ΔU_μ. While ΔU_μ simply depends on the classical potential at the single site of the ion, ΔE_μ is a complicated configurational function taking into account the delocalization of the electron in state R (HOMO) and full electronic relaxation after ET in state O. Straightforward sampling of the equilibrium distribution of ΔE_μ will give rather poor statistics, in particular for the important crossing region. Unfortunately, ΔE_μ cannot be easily controlled in a constrained MD scheme like an ordinary configurational order parameter such as ΔU_μ as it depends also on electronic degrees of freedom. This was one reason why we have chosen ΔU_μ (respectively ϕ) for our constrained MD approach and not ΔE_μ. However, as pointed out by Tachiya [30], the free energy curves can be sampled reasonably well by exploiting Eq. (12) combining data points obtained from two equilibrium simulations of R and O to one diabatic curve.

2.3 Homogeneous electron transfer at infinite separation

The self-exchange reaction:

$$Ru^{*2+} + Ru^{3+} \longrightarrow Ru^{*3+} + Ru^{2+} \tag{28}$$

is a classical example of a homogeneous ET reaction. Rate constants have been determined in aqueous [45] and non-aqueous [46] solutions and calculated from crystallographic [47] and spectroscopic [48] data using the equations of Marcus. Computation of ET rates from first principle simulation that can be directly compared to experimental results still represents a major challenge. One reason is that most ET reactions are well in the nonadiabatic regime (see e.g. Refs. [5, 6]). Since the simulation methodology used here is based on Born–Oppenheimer dynamics it cannot be applied without further approximations (for example surface hopping methods). In addition, density functional-based MD simulation of homogeneous ET is also held back by a more technical complication, namely the self-interaction error of current density functionals incorrectly favouring delocalized states with fractional charge over mixed valence states.

Here we consider homogeneous ET only in a highly idealized limit: donor and acceptor are assumed to be separated by an infinite distance while at the same time the transfer is assumed to be completely adiabatic. These two assumptions are a contradiction which is impossible to realize in experiment. Such an approach, however, is meaningful in Marcus theory which separates the ET rate in an electronic coupling parameter and a Franck–Condon factor. The behaviour of the Franck–Condon factor can thus be studied independently of the effect of the electronic coupling (see for example Refs. [23,25]). It is this Franck–Condon factor which is described in Marcus theory by intersecting diabatic free energy surfaces.

The present calculation must be seen in this context. We use the single ion ab initio approach employed for heterogeneous ET to estimate the free energy profiles for homogeneous ET between two metal ions infinitely far apart. In this limit the motion of donor R of the reactant state A = (R + O) is independent of the acceptor O. The total system can therefore be divided in two subsystems 1 and 2 consisting of the ions R and O. Similarly the product B = (R^+ + O^-) can be resolved in two noninteracting ions $R^+ = O$ and $O^- = R$. The order parameter is then the difference between the ionization energy $\Delta E_0(\mathbf{R}_1^N)$ of subsystem 1 at configuration $\mathbf{R}_1^N$ and the electron affinity $\Delta E_0(\mathbf{R}_2^N)$ of subsystem 2 at configuration $\mathbf{R}_2^N$, yielding an electronic gap $\Delta\Delta E_0$ for transfer:

$$\begin{aligned}\Delta\Delta E_0(\mathbf{R}^{2N}) &= \Delta\Delta E_0(\mathbf{R}_1^N, \mathbf{R}_2^N) \\ &= \Delta E_0(\mathbf{R}_2^N) - \Delta E_0(\mathbf{R}_1^N),\end{aligned} \tag{29}$$

where ΔE_0 is given in Eq. (22). Donor and acceptor ions R and O are uncorrelated at infinite separation, hence the probability distribution of the reactant $p_A(\Delta\Delta E_0)$ is the convolution of the distributions $p_R(\Delta E_0(\mathbf{R}_1^N))$ and $p_O(\Delta E_0(\mathbf{R}_2^N))$ obtained from the single ion MD runs of R and O:

$$\begin{aligned}p_A(\Delta\Delta E_0) = \int_{-\infty}^{\infty} &d\Delta E_0 \; p_R(\Delta E_0) \\ &\times p_O(\Delta E_0 - \Delta\Delta E_0).\end{aligned} \tag{30}$$

The free energy profile of the reactant $A_A(\Delta\Delta E_0)$ is then,

$$A_A(\Delta\Delta E_0) = -k_B T \ln p_A(\Delta\Delta E_0) + A_A. \tag{31}$$

where A_A is a constant. For self-exchange reactions such as Eq. (28) the free energy profile for the product B is given by inversion symmetry:

$$A_B(\Delta\Delta E_0) = A_A(-\Delta\Delta E_0). \tag{32}$$

2.4 Spectral density function of ET energy

For a closer analysis of the dynamics driving the ET we follow Ref. [25] and calculate the TCFs $c_M(t)$ of the ET energy fluctuations:

$$c_M(t) = \langle \delta\Delta E_0(0)\delta\Delta E_0(t)\rangle_M \tag{33}$$

where $\delta\Delta E_0(t) = \Delta E_0(t) - \langle\Delta E_0\rangle_M$, M = R, O. Fourier transformation of $c_M(t)$ gives the spectral density function $J_M(\omega)$ defined as

$$\frac{J_M(\omega)}{\omega} = \frac{\beta}{4}\int_0^{\infty} dt\, c_M(t)\cos\omega t \tag{34}$$

and the inverse returns $c_M(t)$

$$c_M(t) = \frac{8}{\beta\pi}\int_0^{\infty} d\omega\, \frac{J_M(\omega)}{\omega}\cos\omega t. \tag{35}$$

Note that the TCF at $t = 0$ equals the variance of the ET energy fluctuations:

$$c_M(0) = \langle \delta\Delta E_0^2\rangle_M. \tag{36}$$

If we assume that linear response applies we obtain

$$\lambda'_M = \frac{\beta}{2}c_M(0) = \frac{4}{\pi}\int_0^{\infty} d\omega \frac{J_M(\omega)}{\omega} \tag{37}$$

by inserting Eq. (36) into Eqs. (18),(19) ($\Delta E \equiv \Delta E_0$) and using relation Eq. (35). The reorganization free energy can be interpreted as the sum total of the spectral components of the TCF of the ET energy. The relaxation free energy can therefore be partitioned into contributions from different bands with weights proportional to the integral of $J_M(\omega)/\omega$ over the corresponding spectral region.

2.5 Molecular dynamics and electronic structure method

The molecular dynamics and electronic structure method used are described in detail in Ref. [35]. Aqueous solutions of Ru^{3+} and Ru^{2+} are modelled by a periodically replicated cubic cell filled with solvent molecules and a single metal ion. There are no counter ions. The net charge is compensated by a neutralizing homogeneous background. The length of the

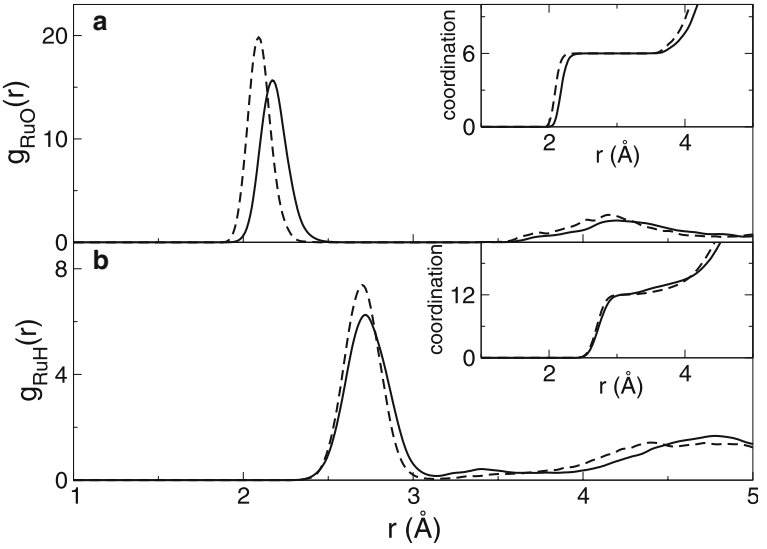

Fig. 1 Metal–oxygen (**a**) and metal–hydrogen (**b**) radial distribution functions of aqueous Ru^{2+} (*solid lines*) and Ru^{3+} (*dashed lines*) obtained from CPMD simulations at 300 K. The solutions are modelled by periodically repeated cubic cells containing one metal ion and 32 water molecules. The *insets* show the oxygen and hydrogen coordination numbers obtained from spherical integration of the corresponding distributions. The data were collected in bins of width 0.01 Å . The distributions were averaged over a trajectory of length 5 ps and smoothed by convolution with a gaussian of width 0.03 Å. Note that both ions are sixfold coordinated with a Ru–O bond length 0.08 Å shorter in the oxidized state

cell was set equal to 9.86 Å , the size for the MD cell of the minimal 32 water molecule model system used in the first simulations of pure liquid water (see e.g. Ref. [49]). The number of solvent molecules was the same as used for the Ag^+ cation simulations of Ref. [33]. It was determined by running a classical simulation of the Ag^+ cation in a large solvent system (256 molecules) and counting the number of water molecules in a cubic box of length 9.86 Å centred on the classical ion [50]. This number, averaged over time, turned out to be close to 32, exactly the same as in the pure liquid. The apparent net zero volume of the solute is a reflection of the contraction of the liquid around the cation due to electrostriction effects (for another example of this procedure see Ref. [36]).

We used the Car–Parrinello method [51] as implemented in the CPMD package [52]. The simulations were carried out using a fictitious mass of 500 a.u., a time step of 5 a.u. (0.1209 fs) and a temperature rescaling to 300 K if the instantaneous temperature exceeded a boundary of 300 ± 50 K. The classical ET energy Eq. (27) was calculated every ten steps and the quantum ET energy Eq. (21) every 50 MD steps along an equilibrium trajectory of length 5 ps. The CPMD simulations of the hexahydrates in vacuum were done similarly. Periodic images were removed using the scheme of Hockney [53]. The pseudo potentials for Ru, O and H were constructed according to the Troullier-Martins scheme [54]. See Ref. [35] for further details. The orbitals were expanded in plane waves with a reciprocal space cutoff of 70 Ry. The exchange-correlation energy was calculated using the generalized gradient approximation (GGA) for exchange according to Becke [55] and the GGA for correlation according to Lee, Yang and Parr [56]. Aqueous solutions and vacuum hydrates of Ru^{2+} (d^6) and Ru^{3+} (d^5) were simulated for the low spin configurations $2S+1=1$ and $2S+1=2$ using the local spin density approximation for Ru^{3+}.

3 Results

3.1 Structural properties

The metal oxygen radial distribution functions of Ru^{2+} and Ru^{3+} are shown in Fig. 1a. Both ions form stable octahedral complexes with average Ru–O bond distances of 2.18 Å for Ru^{2+} and 2.10 Å for Ru^{3+}. The experimental bond length determined for dilute solutions [45] (and crystals [47]) are 2.11 Å (2.122 Å) for the reduced ion and 2.03 Å (2.029 Å) for the oxidized ion. Despite overestimation of the absolute values by about 0.07 Å, the difference of the Ru–O bond length in the two oxidation states, 0.08 Å, is identical to the experimental result [45]. The first peak of the Ru–O distribution is symmetric and rather broad displaying fluctuations in coordination distance of the six ligand water molecules between 1.98–2.53 Å for Ru^{2+} and 1.92–2.40 Å for Ru^{3+}. The radial distribution function vanishes in the range 2.54–3.40 Å, respectively 2.41–3.39 Å, indicating a clear separation between first and second solvation shell. As one can see from Fig. 1a the density increase in the second shell is steeper for Ru^{3+} than for Ru^{2+}, indicating that the response to the increase in charge extends beyond the contraction of the first solvation shell.

In contrast to reduction of the Ru–O bond length, the Ru–H distance does not change significantly upon oxidation of Ru^{2+} to Ru^{3+}. The first maximum of the Ru–H radial distribution function shown in Fig. 1b is located at 2.72 and 2.71 Å for reduced and oxidized states, respectively. The

different response of the metal–oxygen and metal–hydrogen distances is due to variation of the tilt angle τ defined by the Ru–O axis and the axis in the water molecule plane intersecting the bending angle. As illustrated in Fig. 2 the centre of the very broad distribution of τ is shifted from roughly 48° for Ru^{2+} to about 40° for Ru^{3+} keeping the average Ru-H distance almost unchanged. Tilt angles in the range 30–70° are not unusual for aqueous cations and have been observed in experiment [57]. Previous simulation studies generally find water molecules in the first hydration of trivalent cations, to be tilted as well but over smaller angles ($< 30°$, [37–41]).

Deviation from radial coordination is a consequence of orbital interactions between metal ion and water ligands as well as hydrogen bonding to neighbouring molecules [57]. Martinez and coworkers give an interesting purely electrostatic argument for the tilt angles observed in a semi-continuum study of aqueous Ag^+ [58]. This tilt is a direct consequence of the interaction with the reaction field describing the polar solvent (see also Ref. [59]). The distortion of the water ligands leads to an increase of the multipole moments of the complex which increases the interaction with the bulk solvent [60,61]. With increasing tilt angle the ion water-dipole interaction becomes less favorable, however, which is particularly important for highly charged and small cations. This argument could also explain the shift of the tilt angle distribution of Ru^{3+} to smaller values when compared to Ru^{2+}.

Size effects of the radial distribution functions are minor. The position of the peak maxima for the 16, 32 and 50 water molecule systems investigated varies by not more than 0.01 Å which is in the order of the statistical uncertainties. However, the average Ru-O distance of the 32 water molecule model solutions of Ru^{2+} and Ru^{3+} are shifted by 0.04 and 0.03 Å to larger distances wrt. average bond lengths of hexahydrates in vacuum at $T = 300$ K. In general bulk solvation is found to reduce the metal oxygen distance compared to the zero temperature vacuum clusters [37,39–41]. Our results for Ru seem to be somewhat of an exception in this respect which requires an explanation. Unfortunately the trends predicted by continuum models are not entirely conclusive. Depending on whether a spherical or a molecular shape cavity is used, the metal oxygen bond length either expands or shrinks with respect to the isolated hexahydrate value [62]. In Ref. [58] it was argued, on the basis of an electrostatic picture, that second shell ligands and bulk molecules have opposite effects on metal–oxygen bonding distances. Our results suggest that Ru^{2+} and Ru^{3+} could be an example of an ion where the balance is the other way around leading to an expansion of the metal–oxygen distances in the first shell.

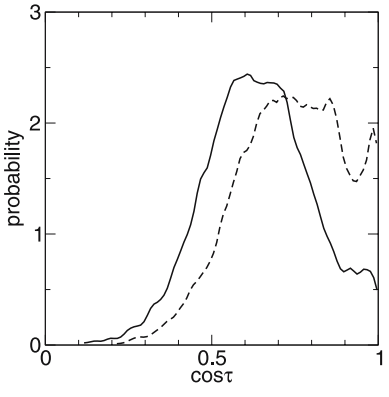

Fig. 2 Tilt angle distribution for the six first shell water molecules coordinated to Ru^{2+} and Ru^{3+} as obtained from CPMD runs at 300 K (system as in Fig. 1). The tilt angle is defined by the plane of the water molecule and the Ru–O axis. At $\tau = 0°$ the water molecule plane contains the Ru–O axis as required for T_h symmetry. The data were collected in bins of width 0.01. The distributions were averaged over 5 ps and smoothed with a gaussian window of width 0.01

A comparison to the results of zero temperature ab initio calculations in the gas phase may be of interest as well. The average bond lengths we obtain for the solvated ions of Ru^{2+} and Ru^{3+} are similar to the values for the hexahydrates in vacuum (0 K), 2.197 and 2.090 Å, computed from symmetry restricted optimizations at the CASSCF level [63]. In this study, too, the Ru–O bond lengths of both oxidation states are overestimated by about 0.06–0.08 Å wrt. experiment (solution and crystal) resulting in a reasonably good estimate for the relative difference. A somewhat better agreement with the experimental absolute bonding distance has been obtained in the DFT study of Ref. [64] for $Ru(H_2O)_6^{3+}$, 2.044 Å. At 300 K the average MD bond length of $Ru(H_2O)_6^{3+}$, 2.07 Å, is mid way between the values obtained in Refs. [63], [64]. The interpretation of geometry optimization in vacuum is however not without ambiguity. The reason is that, similar to the solvated complex, also the Ru^{2+} vacuum cluster shows distinct anomalous behaviour according to our calculations. Unlike most hexahydrates of ions with spherical closed shell electronic configurations (so excluding Jahn Teller complexes) the equilibrium geometry of Ru^{2+}, as obtained in our plane wave pseudo potential code, deviates from the familiar T_h structure. The coordinated water molecules already show an appreciable tilt ($\tau = 46°$ for Ru^{2+} and $\tau = 38°$ for Ru^{3+}) even without the presence of a second solvation shell. This result was verified by repeating the calculation using the ADF code [65] yielding similarly large tilt angles ($\tau = 41°, 28°$ for Ru^{2+} respectively Ru^{3+}). As also suggested in Ref. [59] tilting of the molecular plane and stretching of the metal–oxygen bond are most likely coupled, which could provide another mechanism for the observed dilation of the metal to oxygen distance in solution.

3.2 Free energy profiles for heterogeneous ET

The probability distributions Eq. (4) of quantum and classical ET energy, ΔE_μ [Eq. (21)] and ΔU_μ [Eq. (27)] are shown in Figs. 3a and 4a, respectively. Both distributions were calculated from 5 ps of equilibrium CPMD runs for oxidized (O) and reduced (R) state at 300 K for the model system consisting of 32 solvent molecules. The electronic chemical potential $\mu = 0.58$ eV was chosen to equal $-\Delta A$ obtained from Eq. (24). For this particular value of μ the minima of the

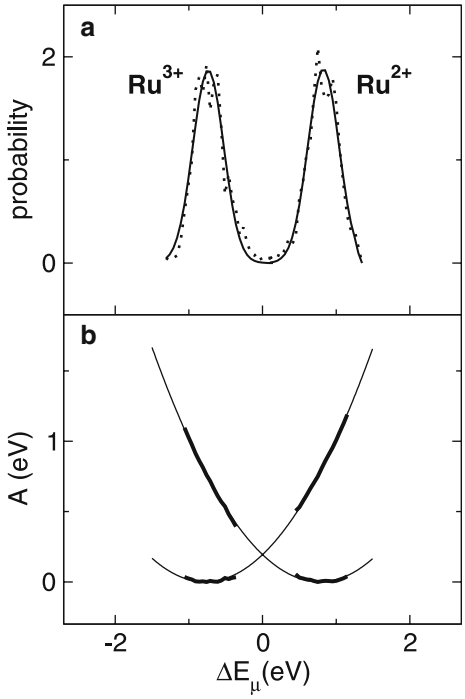

Fig. 3 Equilibrium distributions of the quantum ET energy [vertical energy gap, Eq. (21)] ΔE_μ (**a**) and the corresponding diabatic free energy profiles (**b**) for the redox couple Ru^{2+}/Ru^{3+}. The probability distributions Eq. (4) ($\xi = \Delta E_\mu$) obtained from equilibrium CPMD simulations of Ru^{2+} and Ru^{3+} are shown in *dotted lines*. Gaussian fits are indicated in *solid lines*. Data points within 1.5 standard deviations from the centre of the distributions were used to obtain the two lower branches of the free energy profiles (*thick lines*). The upper branches (*thick lines*) were obtained from the lower branches using the linear free energy relation Eq. (12). For each state lower and upper branch are fitted to a parabola (*thin lines*) giving the full diabatic free energy curve for Ru^{2+} and Ru^{3+}, respectively. The electronic chemical potential was chosen so that the minima of the diabatic curves are aligned

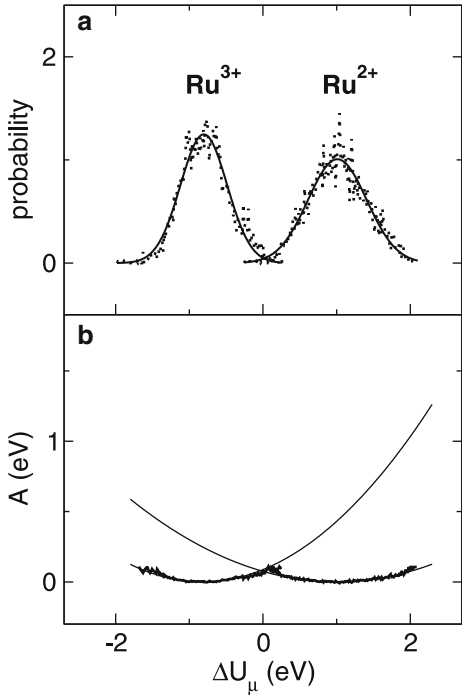

Fig. 4 Equilibrium distributions of the classical ET energy [solvent electrostatic potential, Eq. (27)] ΔU_μ (**a**) and diabatic free energy curves (**b**) for the redox couple Ru^{2+}/Ru^{3+}. The probability distribution Eq. 4 ($\xi = \Delta U_\mu$, *dotted lines*) are obtained from equilibrium CPMD simulations of Ru^{2+} and Ru^{3+} and taken from Ref. [35]. Gaussian fits are indicated in *solid lines*. The corresponding free energy curves (*thick lines* in **b**) are fitted to parabolae (*thin lines*). The electronic chemical potential was chosen so that the minima of the diabatic curves are aligned. The scale of the axes was chosen equal to the one in Fig. 3 to emphasize the difference in fluctuation of quantum and classical ET energy

two free energy curves are aligned, $\Delta A_\mu = 0$. The fluctuations of the two coordinates ΔE_μ and ΔU_μ are well approximated by gaussian distributions for both oxidation states with correlation coefficients of about 0.98. The corresponding diabatic free energy curves using ΔE_μ as order parameter (Fig. 3b) are constructed by combining the data points obtained from equilibrium simulation of R and O. The lower right branch of the curve for R is obtained from the equilibrium distribution of R. The upper left branch of the curve for R is obtained from the equilibrium distribution of O and shifted according to Eq. (12) by $-\Delta E_\mu$. Both upper and lower curves are fitted to one parabola giving the diabatic free energy profile for state R. The profile for state O is constructed similarly. This procedure of combining data points has not been applied to the curves along ΔU_μ because the linear free energy relation Eq. 12 is not valid for ΔU_μ. However, the curves shown in Fig. 4b have been confirmed in Ref. [35] using constrained MD.

As one can see in Fig. 3b the quadratic fit functions in ΔE_μ approximate the data points very well (correlation coefficient of 0.9998). The curvature is equal for both states and the position of the minimum coincides with the reorganization free energy as predicted by Eqs. (15) and (16) ($\Delta A \equiv \Delta A_\mu = 0$, see Table 1). The Ru^{2+}/Ru^{3+} redox couple is therefore very well described by the linear response approximation. A striking observation is that the distributions of the classical ET energy ΔU_μ are also gaussian but significantly broader compared to ΔE_μ and distinctly asymmetric. Contrary to ΔE_μ the linear free energy relation Eq. (12) does not apply for ΔU_μ, therefore imposing no constraints on the relative values of the widths of gaussian distributions for ΔU_μ. In fact, the reorganization free energy in the oxidized state is almost twice as large as for the reduced state. Our results suggest therefore that electronic ionization and relaxation effects that are missing in the classical potential but fully represented in the electronic energy gap lead to smaller and symmetric fluctuations of the corresponding ET energy.

A further test for 'Marcus' type free energy curves is provided by Eqs. (18), (19) and (20) which relate the reorganization free energy to the variance of order parameter fluctuations. Equation (20) is exact for two parabolae with equal curvature that obey the linear free energy relation Eq. (12). For ΔE_μ the agreement between λ'_M and λ_M is reasonably good, $\lambda'_M = 1.0\,\text{eV}$, $\lambda_M = 0.8\,\text{eV}$, M=R,O. The small discrepancy

Table 1 Equilibrium distribution and free energy profile for quantum [$\xi = \Delta E_\mu$, Eq. (21)] and classical [$\xi = \Delta U_\mu$, Eq. (27)] electron transfer (ET) energy of the single ions Ru^{2+} (R) and Ru^{3+} (O) in solution and vacuum

	Solution		Vacuum	
	Quantum	Classical	Quantum	Classical
$\langle\xi\rangle_R$ (eV)	0.81	1.02	0.66	0.37
$\langle\xi\rangle_O$ (eV)	−0.70	−0.78	−1.01	−0.46
$\langle\delta\xi^2\rangle_R^{1/2}$ (eV)	0.225	0.386	0.277	0.352
$\langle\delta\xi^2\rangle_O^{1/2}$ (eV)	0.227	0.326	0.219	0.316
λ_R (eV)	0.78	0.24	0.82	0.08
λ_O (eV)	0.78	0.42	0.83	0.09
ξ_R (eV)	0.78	1.00	0.84	0.35
ξ_O (eV)	−0.78	−0.82	−0.82	−0.47
λ'_R (eV)	0.98	2.88	1.48	2.40
λ'_O (eV)	1.00	2.06	0.93	1.93
ΔA (eV)	−0.58	10.34	11.37	21.27
ΔA_μ (eV)	0	0	0	0
$\Delta A_\mu^\ddagger$ (eV)	0.20	0.08	0.21	0.02

The solutions are modelled by a periodically repeated unit cell containing one ion and 32 water molecules. The ion in vacuum is coordinated by six water molecules and treated as isolated system. $\langle\xi\rangle_M$ and $\langle\delta\xi^2\rangle_M^{1/2}$ denote average and width of the distributions Eq. (4) obtained from CPMD runs in state M, M = R,O, at 300 K. For evaluation of ΔU_μ we have used the SPC charges for O and H atoms, $q_O = -2q_H = -0.8476e$, $\Delta E_0^v = 28.7$ eV [36] and $q_O = 3$, $q_R = 2$. The finite size correction (second term on the RHS of Eq. 26) was omitted for calculations in vacuum. λ_M is the relaxation free energy of Eqs. (7) and (8) obtained from the parabolic fit of the free energy curves shown in Figs. 3b and 4b. The position of the minimum of the parabolic fits is denoted ξ_M. λ'_M is obtained from $\langle\delta\xi^2\rangle_M$ according to Eqs. (18) and (19). $\Delta A_\mu^\ddagger$ denotes the solvation free energy barrier obtained from the crossing point of the parabolic fits

is due to the fact that λ_M is obtained from a fit combining the data points of states R and O while λ'_M is obtained separately for each state. Therefore λ_M has smaller statistical uncertainty than λ'_M and is the preferred value. These relations are unique to the true energy gap and, for a quantum system, no longer hold for the classical solvent electrostatic energy ΔU_μ. This is illustrated by the large deviation between the classical reorganization free energies λ'_M and λ_M where λ'_M was obtained by replacing $\delta\Delta E$ with $\delta\Delta U$ in Eqs. (18) and (19) (see Table 1).

The reorganization free energy is usually partitioned in contributions from the inner sphere consisting of the ion + first shell ligands and the outer sphere consisting of solvent molecules. These energy components can be easily determined in classical MD simulations because the contribution of single water molecules to the classical ET energy is explicitly known. Such an energy decomposition is more difficult for the quantum ET energy requiring special localization methods which have not been implemented in our code. A first estimate of the outer sphere contribution can however be obtained by comparing the relaxation free energies in solution with those computed from a simulation of the first shell coordination complex in vacuum.

The ET energy distributions obtained for the ruthenium hexahydrates in vacuum are again close to gaussian with correlation coefficients similar to the values in solution. Upon solvation the magnitude of the classical ET energy averages is increased (from 0.37 to 1.02 eV for R and from −0.46 to −0.78 eV for O) and also the widths (from 0.352 to 0.386 eV for R and from 0.316 to 0.326 eV for O). This leads to an outer sphere contribution of 66.7 and 78.6% for the reorganization free energies of R and O, respectively (see Table 2). For the quantum ET energy the situation is, however, somewhat confusing. The vacuum free energy curves obtained from combining the data of state O and R fit very well to parabolae. However, the corresponding reorganization free energy in vacuum is not smaller but even larger (0.82 eV) than in solution (0.78 eV) which would imply that the outer sphere contribution is slightly negative. Underestimation of outer sphere contributions can easily be blamed on the small rigid MD cell used in our simulation, frustrating relaxation of long range electrostriction forces (for further discussion of size effects see Sect. 4). However, a negative value of a quantity that is inherently positive, is more difficult to understand. A further consideration in an attempt to rationalize this counterintuitive result could be the observation that in vacuum the metal–oxygen bond lengths of R and O are shorter than in solution (see Sect. 3.1) suggesting that the decrease in free energy as a result of reorganization of the inner sphere complex (hexahydrate) is less severe in solution than in vacuum. If this difference is comparable to the reorganization free energy of the outer sphere water molecules the total reorganization free energy in solution can be equal or even smaller than the value in vacuum. In other words, the vacuum reorganization free energy is a poor approximation to the 'true' inner sphere contribution in solution and our simple-minded partitioning scheme fails for the quantum case.

3.3 Free energy profile for homogeneous ET

As explained in Sect. 2.3 the ET energy distribution for half reactions can be converted to a hypothetical distribution for homogeneous ET in the limit of infinite ion separation [Eq. (30)]. The convolution of quantum and classical ET energy distributions of donor (R) and acceptor (O) yields almost exact gaussian distributions for the energy gap coordinate $\Delta\Delta E_0$ and $\Delta\Delta U_0$, respectively, with correlation coefficients of 0.998 and 0.9999 (see Figs. 5a and 6a and Table 3). As illustrated in Figs. 5b and 6b the free energy curves for the quantum and classical gap are almost perfectly harmonic. The free energy profiles of reactant (Ru^{*2+}–Ru^{3+}, State A, see Section 2) and product (Ru^{*3+}–Ru^{2+}, State B) automatically satisfy Eq. (13) due to symmetry of inversion of the gap [Eq. (32)]. The position of the minimum of the curve for homogeneous ET along the quantum gap is shifted to approximately twice the value for heterogeneous ET, $\xi_A = -\xi_B \approx 2\xi_R \approx -2\xi_O$, and the variance of the fluctuations (second moment) is almost doubled as well $\sigma_A^2 = \sigma_B^2 \approx 2\sigma_R^2 \approx 2\sigma_O^2$. These relations are exact if donor and acceptor distributions are gaussians of equal width (property of the convolution). As a result, also the reorganization free

Table 2 Partition of the single ion reorganization free energy λ_M in inner and outer sphere contributions, f_i and f_o, respectively, and of λ'_M in spectral components, M = R,O

	λ_R		λ_O		λ	
	Quantum	Classical	Quantum	Classical	Quantum	Classical
f_i	105.1	33.3	106.4	21.4	109.9	24.6
f_o	−5.1	66.7	−6.4	78.6	−9.9	75.4
	λ'_R		λ'_O			
0–1,300 cm^{-1}	90.8	95.1	89.9	86.6		
1,300–2,800 cm^{-1}	9.2	4.0	10.1	12.0		
2,800–4,000 cm^{-1}	–	0.9	–	1.4		

λ is the reorganization free energy for homogeneous ET between two infinitely separated ions given in Table 3. The inner sphere contribution is defined as $f_i = \lambda_M(\text{vacuum})/\lambda_M(\text{solution}) * 100$ where λ_M was taken from Table 1, $f_o = 100 - f_i$. The partitioning of λ was done similarly. The relative spectral contributions for λ'_M were obtained by integrating the weighted spectral density function $J(\omega)/\omega$ according to Eq. (37) over the corresponding bands and dividing by λ'_M (see insets of Fig. 8)

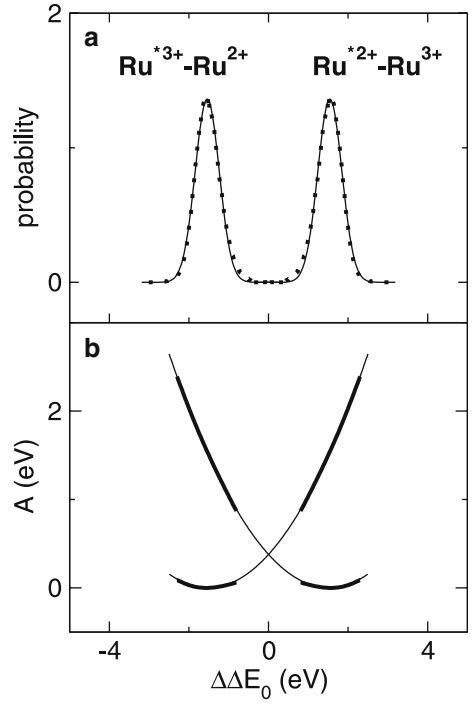

Fig. 5 Equilibrium distributions of the quantum gap energy $\Delta\Delta E_0$ (**a**) and corresponding diabatic free energy profiles (**b**) for the ion pair Ru^{2+}–Ru^{3+} at infinite ion separation. The probability distributions (*dotted lines*) were obtained by convolution of the single ion distributions p_R and p_O [Eq. (30)] shown in Fig. 3a. Gaussian fits of the distributions are displayed in *solid lines*. The distributions and free energy curves are symmetric due to Eq. (32). Data points within 2.5 standard deviations from the centre of the distribution were taken to construct the lower branch of the free energy curve. The upper branch was obtained using the linear free energy relation Eq. (12). Upper and lower branches (*thick lines*) are fitted to parabolae (*thin lines*)

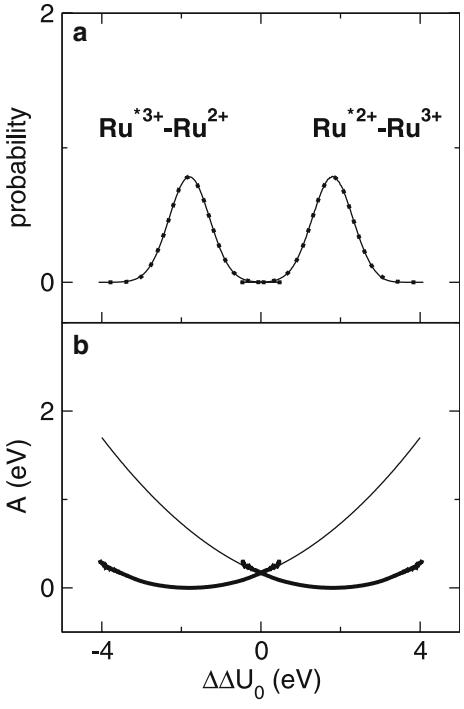

Fig. 6 Equilibrium distributions of the classical gap energy $\Delta\Delta U_0$ (**a**) and the corresponding free energy curves (**b**) for the ion pair Ru^{2+}–Ru^{3+} at infinite ion separation. The probability distributions (*dotted lines*) were obtained by convolution of the single ion distributions p_R and p_O [Eq. (30)] shown in Fig. 4a. Gaussian fits are displayed in *solid lines*. The distributions and free energy curves are symmetric due to Eq. (32). The free energy profiles obtained from the equilibrium distributions (*thick lines*) are fitted to parabolae (*thin lines*)

energy λ increases by a factor 2 (Eqs. 18, 19, 20) and hence also the activation, since $\Delta A^{\ddagger} = \lambda/4$ is predicted to be twice as large as for heterogeneous ET. This result is intuitive since for homogeneous ET both metal ions (and not only one as in heterogeneous ET) have to be thermally excited to form the transition state. From the parabolic fits of our simulation results in solution (Tables 1 and 3) we obtain $\lambda = 1.94\lambda_M$, M = R,O, and $\Delta A^{\ddagger} = 1.90\Delta A^{\ddagger}_{\mu}$ ($\mu = 0.58$ eV) for the quantum gap as order parameter. The deviations from the expected factor 2 must be attributed to small non-gaussian contributions to the equilibrium fluctuations. Solvation effects on the homogeneous ET curves are similar to the ones discussed for heterogeneous ET. While negative for the quantum reorganization free energy, the outer sphere contribution for the

Table 3 Equilibrium distribution and free energy profile for quantum ($\xi = \Delta\Delta E_0$) and classical ($\xi = \Delta\Delta U_0$) gap energy Eq. (29) computed for the infinitely separated ion pair Ru^{2+}-Ru^{3+} in solution and vacuum

	Solution		Vacuum	
	Quantum	Classical	Quantum	Classical
$\langle\xi\rangle$ (eV)	1.54	1.80	1.67	0.82
$\langle\delta\xi^2\rangle^{1/2}$ (eV)	0.303	0.511	0.347	0.466
λ (eV)	1.51	0.65	1.66	0.16
ξ_A (eV)	1.52	1.79	1.67	0.83
λ' (eV)	1.78	5.05	2.33	4.20
ΔA (eV)	0	0	0	0
$\Delta A^{\ddagger}$ (eV)	0.38	0.16	0.41	0.04

$\langle\xi\rangle$ and $\langle\delta\xi^2\rangle_M^{1/2}$ denote average and width of the distribution p_A obtained from convolution of the single ion distributions according to Eq. (30). λ is the relaxation free energy and ξ_A the position of the minimum of the parabolic fit of the free energy curve A_A shown in Figs. 5b and 6b. $\lambda' = \beta\langle\delta\xi^2\rangle/2$. $\Delta A^{\ddagger}$ denotes the activation free energy for homogeneous ET obtained from the crossing point of the parabolic fits. Note that free energy profiles for reactant A and product B are symmetric [Eq. (32)]

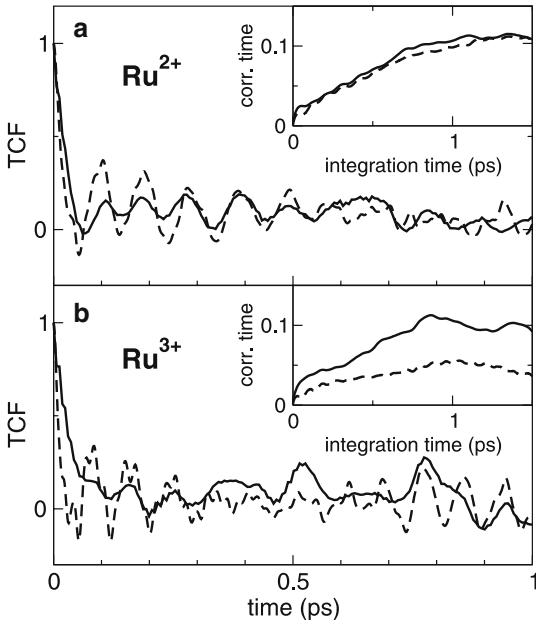

Fig. 7 Normalized time correlation function (TCF) $c_M(t)/c_M(0)$ of quantum and classical ET energy, ΔE_0 (*solid lines*) and ΔU_0 (*dashed lines*), respectively. The TCF is computed from 5 ps equilibrium trajectories of aqueous Ru^{2+} (**a**, M = R) and Ru^{3+} (**b**, M = O) at 300 K. ΔE_0 was sampled every 6 fs and ΔU_0 every 1.2 fs. The *insets* show the integral of the TCF (correlation time) as a function of the integration time

classical reorganization free energy amounts to 75.4% which is close to the estimate obtained in Ref. [25] for the Fe^{2+}–Fe^{3+} system (72% at an ion–ion separation distance $d = 9$ Å).

How well does the estimate for the solvation free energy barrier $\Delta A^{\ddagger} = 0.38$ eV compare to experimental results? According to the measurements of Ref. [46] the rate constant for ET between Ru^{2+} and Ru^{3+} is $k_{obs} = 60 \pm 40\,M^{-1}s^{-1}$. Taking a value of $K_0 = 0.033\,M^{-1}$ [45] for the pre-equilibrium constant and assuming unity for the electronic factor, $\kappa = 1$, the transition state formula $k_{obs} = K_0\kappa\,(kT/h)\exp(-\Delta G^{\ddagger}/RT)$ gives an experimental estimate $\Delta G^{\ddagger} = 0.55$ eV. Our result underestimates the experimental barrier by 0.17 eV and probably by more if calculated for the optimum ion–ion distance and not for the limit of infinite separation. The underestimation is most likely due to the small system size used (see further Sect. 4).

3.4 Spectral analysis of ET energy fluctuations

The normalized TCF $c_M(t)/c_M(0)$ [Eq. 33)] of ΔE_0 and ΔU_0 are shown in Fig. 7 for reduced and oxidized state. The TCFs decay rapidly and cross the zero point after about 50 fs (except for ΔE_0 of O). The oscillations of the TCF of ΔE_0 and ΔU_0 are in phase but the magnitude for ΔU_0 is significantly larger. High frequency components are not resolved in the TCF of ΔE_0 because the quantum ET energy was sampled every 50 MD steps (= 6 fs), only, limiting the maximum frequency to 2,757 cm^{-1}. Contributions from intramolecular motions of water molecules are resolved in the TCF of the classical ET energy which was sampled every 10 MD steps on the same trajectory. After 1 ps the integral of the TCF (correlation time) reaches a plateau value of about 110 fs which is close to its oscillation period. The TCF of ΔU_0 of O decays exceptionally fast leading to a lower correlation time of about 55 fs. Integration of the TCF beyond 1.5 ps gives a sharp decrease of the correlation time due to the finite length of the trajectories (5 ps). We have taken the first 1.5 ps of the TCF for the computation of the spectral density function $J(\omega)$ defined in Eq. (34).

The frequency spectrum of the TCF is shown in Fig. 8 for reduced and oxidized state. Quantum and classical ET energy fluctuations of Ru^{2+} are dominated by the Ru–O deformation modes between 0–500 cm^{-1}. Somewhat surprisingly, the quantum ET energy fluctuations do not exhibit significant intensity at higher frequencies. This is in contrast to the classical fluctuations which show a broad band between 500–1,100 cm^{-1} (Ru–O stretch, H_2O rocking, twisting,...) and two sharp peaks at around 1,580 cm^{-1} (H_2O bending). Contributions from intramolecular OH bond stretching are minor. The spectrum for Ru^{3+} is blue shifted in the region 0–500 cm^{-1} wrt. the spectrum of Ru^{2+}. This is in agreement with our expectation as ion–ligand vibrational frequencies usually increase with increasing ion charge. The difference between spectra of quantum and classical ET energy fluctuations is again striking for frequencies higher than 500 cm^{-1}. While for the quantum fluctuations virtually no intensity is observed, the classical fluctuations show sharp peaks of high intensity at around 910 and 1,560 cm^{-1}. Thus, electronic relaxation seems to compensate the ET energy fluctuations arising from high frequency motions of ligand and solvent molecules. The pronounced difference of spectra in the bending region is not reflected in the spectral decomposition of the reorganization free energy λ'_M (Table 2). The

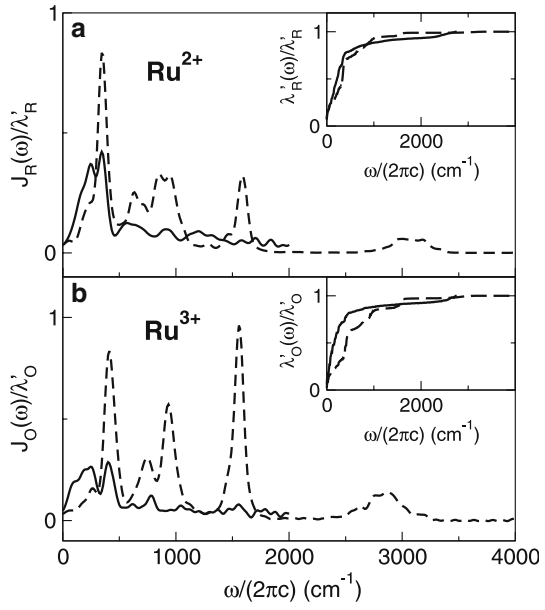

Fig. 8 Spectral density function J_M of quantum and classical ET energy, ΔE_0 (*solid lines*) and ΔU_0 (*dashed lines*), respectively, obtained for aqueous Ru^{2+} (**a**, M=R) and Ru^{3+} (**b**, M=O). $J_M(\omega)$ was evaluated by Fourier transformation of the corresponding TCFs shown in Fig. 7 according to Eq. (34). The *insets* display the integral $\lambda'_M(\omega)/\lambda'_M = 4/\pi \int_0^\omega \mathrm{d}\omega' J_M(\omega')/(\lambda'_M\omega')$ where λ'_M is defined in Eq. (37). The maximum frequency resolved for ΔE_0 is 2,757 cm^{-1} corresponding to a sampling interval of 6 ps (shown for the range 0–2,000 cm^{-1}). The resolution of the spectra is 11.1 cm^{-1} for ΔE_0 and ΔU_0. The spectra were convoluted with a gaussian window of width 30 cm^{-1}

contributions are similar for quantum and classical ET energy because the weight factor $1/\omega$ in Eq. (37) smears out the difference of intensities for higher frequencies. About 90% of the fluctuations are due to the slow metal–oxygen vibrations and only 10% due to bending motion while contributions from intramolecular stretching modes are minor.

4 Discussion and conclusion

In this work we have compared the free energy profiles for the redox reaction between Ru^{2+} and Ru^{3+} using two different order parameters: the quantum and classical energies, respectively required to transfer an electron from Ru^{2+} to an idealized noninteracting electrode. We found that the diabatic curves for both coordinates are well approximated by quadratic functions. The horizontal position of the free energy minima are similar for both coordinates but the curvature along the classical coordinate is significantly smaller and asymmetric. As electronic polarization is missing in the classical ET energy, this difference must be a consequence of the delocalization of the HOMO over first shell ligands and electronic relaxation after ET. The net effect is a decrease of fluctuations of the energy gap between the two diabatic states and therefore an increased curvature of the free energy profile. The reorganization free energies of Ru^{3+} and Ru^{2+} that differ by a factor of almost 2 for the classical coordinate become equal if the electronic relaxation is explicitly considered.

This, at first, somewhat surprising result seems to suggest that the effect of an oxidation state dependence of solute polarizability is opposite to what was intended by the Matyushov–Voth model [31,21]. Rather than enhancing the difference between oxidation states, the electronic polarizability of solute (and solvent) apparently smoothes out these differences, bringing the ions back to the linear regime. For a proper interpretation of this statement we should make two qualifications. First we recall the results of Ref. [12] showing that a fully classical model of the solution, in which the solvent electrostatic potential (which we indicated by ΔU_μ) is identical to the energy gap, indeed produces free energy curves for the two oxidation states with almost equal curvature, similar to the electronic structure calculations reported here. This suggests that the asymmetry that we found when the same classical order parameter is applied in a DFT simulation, is probably due to the inconsistency in the treatment of electronic polarization, which is included in the molecular dynamics but not in the classical gap energy.

Secondly there remains, of course, the crucial question to what extent these observations are caused by the very limited system size dimension of our models. Indeed the size dependence of the reorganization free energy (λ) is large. It can be shown that the error in λ as computed using a classical model of the Fe^{2+} and Fe^{3+} aqua ions is inversely proportional to the box length (L), adding easily an eV or more to the estimate obtained from a model as small as used here (32–50 solvent molecules). As almost all of the increase with system size will come from the expansion of the outer shell the problem of the negative contribution of this region to the reorganization in a small system (Table 2) will disappear. Since the system can however be assumed to stay in the linear regime when scaled up, our main result can be safely generalized to all system sizes. We conclude therefore that the predictions of Marcus theory apply very well to the Ru^{2+}/Ru^{3+} redox couple provided that the 'correct' Marcus order parameter is taken as reaction coordinate. For ab initio MD simulations this is the quantum ET energy.

Acknowledgements This research was sponsored by EPSRC. JB is grateful to the Austrian Academy of Sciences for financial support. We also acknowledge the helpful discussions with Masanori Tachiya. The bulk of the computations was carried out on the HPCx facility at Daresbury.

References

1. Marcus RA (1956) J Chem Phys 24:966
2. Marcus RA (1960) Discuss Faraday Soc 29:21
3. Marcus RA (1965) J Chem Phys 43:679
4. Marcus RA (1993) Rev Mod Phys 65:599
5. Jortner J, Bixon M (eds) (1999) Electron transfer – from isolated molecules to biomolecules. Adv Chem Phys 106:107
6. Barzykin AV, Frantsukov PA, Seki K, Tachiya M (2002) Adv Chem Phys 123:511

7. Warshel A (1982) J Phys Chem 86:2218
8. Hwang JK, Warshel A (1987) J Am Chem Soc 109:715
9. King G, Warshel A (1990) J Chem Phys 93:8682
10. Kuharski RA, Bader JS, Chandler D, Sprik M, Klein ML, Impey RW (1988) J Chem Phys 89:3248
11. Carter EA, Hynes JT (1989) J Phys Chem 93:2184
12. Rose DA, Benjamin I (1994) J Chem Phys 100:3545
13. Rose DA, Benjamin I (1995) Chem Phys Lett 234:209
14. Yelle RB, Ichiye Y (1997) J Phys Chem B 101:4127
15. Straus JB, Voth GA (1993) J Phys Chem 97:7388
16. Straus JB, Calhoun A, Voth GA (1995) J Chem Phys 102:529
17. Calhoun A, Voth GA (1996) J Phys Chem 100:10746
18. Calhoun A, Voth GA (1998) J Phys Chem B 102:8563
19. Calhoun A, Koper MTM, Voth GA (1999) J Phys Chem B 103:3442
20. Calhoun A, Koper MTM, Voth GA (1999) Chem Phys Lett 305:94
21. Small DW, Matyushov DV, Voth GA (2003) J Am Chem Soc 125:7470
22. Ando K, Kato S (1991) J Chem Phys 95:5966
23. Ando K (1997) J Chem Phys 106:116
24. Ando K (2001) J Chem Phys 114:9040
25. Ando K (2001) J Chem Phys 114:9470
26. Hartnig C, Koper MTM (2001) J Chem Phys 115:8540
27. Hartnig C, Koper MTM (2003) J Am Chem Soc 125:9840
28. Kakitani T, Mataga N (1985) J Phys Chem 89:8
29. Kakitani T, Mataga N (1985) Chem Phys 93:381
30. Tachiya M (1989) J Phys Chem 93:7050
31. Matyushov DV, Voth GA (2000) J Chem Phys 113:5413
32. Bard AJ, Faulkner LR (eds) (2001) Electrochemical Methods. 2nd ed, Wiley, London
33. Blumberger J, Bernasconi L, Tavernelli I, Vuilleumier R, Sprik M (2004) J Am Chem Soc 126:3928
34. Blumberger J, Sprik M (2004) J Phys Chem B 108(21):6529
35. Blumberger J, Sprik M (2005) J Phys Chem B 109:6793
36. Tateyama Y, Blumberger J, Sprik M, Tavernelli I (2005) J Chem Phys 122:234505
37. Wasserman E, Rustad JR, Xantheas SS (1997) J Phys Chem 106:9769
38. Ikeda I, Hirata M, Kimura T (2003) J Chem Phys 119:12386
39. Spångberg D, Hermansson K (2004) J Phys Chem 120:4829
40. Amira S, Spångberg D, Zelin V, Probst M, Hermansson K (2005) J Phys Chem B 109:14235
41. Martinez JM, Pappalardo RR, Sánchez Marcos E (1998) J Chem Phys 109:1445
42. Zwanzig RW (1954) J Chem Phys 22:1420
43. Tavernelli I, Vuilleumier R, Sprik M (2002) Phys Rev Lett 88:213002
44. Hummer G, Pratt LR, Garcia AE (1998) J Phys Chem A 102:7885
45. Brunschwig BS, Creutz C, McCartney DH, Sham TK, Sutin N (1982) Faraday Discuss Chem Soc 74:113
46. Böttcher W, Brown GM, Sutin N (1979) Inorg Chem 18:1447
47. Bernhard P, Bürgi H-B, Hauser J, Lehmann H, Ludi A (1982) Inorg Chem 21:3936
48. Bernhard P, Ludi A (1984) Inorg Chem 23:870
49. Sprik M, Hutter J, Parrinello M (1996) J Chem Phys 105:1142
50. Vuilleumier R, Sprik M (2001) J Chem Phys 115:3454
51. Car R, Parrinello M (1985) Phys Rev Lett 55:2471
52. Hutter J, Ballone P, Bernasconi M, Focher P, Fois E, Goedecker St, Marx D, Parrinello M, Tuckerman M (1998) CPMD version 3.3, MPI für Festkörperforschung and the IBM Zurich Research Laboratory
53. Hockney RW (1970) Methods Comput Phys 9:136
54. Troullier N, Martins (1991) J Phys Rev B 43:1993
55. Becke AD (1988) Phys Rev A 38:3098
56. Lee C, Yang W, Parr R (1988) Phys Rev B 37:785
57. Ohtaki H, Radnai T (1993) Chem Rev 93:1157
58. Martinez JM, Pappalardo RR, Sánchez Marcos E (1997) J Phys Chem A 101:4444
59. Jarzeçki AA, Anbar AD, Spiro TG (2004) J Phys Chem A 108:2726
60. Karlström G (1988) J Phys Chem 92:1318
61. Bertran J, Ruiz-Lopez MF, Rinaldi D, Rivail JL (1992) Theor Chim Acta 84:181
62. Martinez JM, Pappalardo RR, Sánchez Marcos E, Mennucci B, Tomasi J (2002) J Phys Chem B 106:1118
63. Akesson R, Pettersson LGM, Sanström M, Wahlgren U (1994) J Am Chem Soc 116:8691
64. Rosso KM, Rustad JR, Gibbs GV (2002) J Phys Chem A 106:8133
65. ADF2002.03, SCM, `http://www.scm.com` (2002) Theoretical Chemistry, Vrije Universiteit, Amsterdam, The Netherlands